

# Scaling exponents for a monkey on a tree: Fractal dimensions of randomly branched polymers

Hans-Karl Janssen

*Institut für Theoretische Physik III, Heinrich-Heine-Universität, 40225 Düsseldorf, Germany*

Olaf Stenull\*

*Department of Physics and Astronomy, University of Pennsylvania, Philadelphia, Pennsylvania 19104, USA*

(Received 13 March 2012; published 17 May 2012)

We study asymptotic properties of diffusion and other transport processes (including self-avoiding walks and electrical conduction) on large, randomly branched polymers using renormalized dynamical field theory. We focus on the swollen phase and the collapse transition, where loops in the polymers are irrelevant. Here the asymptotic statistics of the polymers is that of lattice trees, and diffusion on them is reminiscent of the climbing of a monkey on a tree. We calculate a set of universal scaling exponents including the diffusion exponent and the fractal dimension of the minimal path to two-loop order and, where available, compare them to numerical results.

DOI: [10.1103/PhysRevE.85.051126](https://doi.org/10.1103/PhysRevE.85.051126)

PACS number(s): 64.60.ae, 05.40.-a, 64.60.Ht

## I. INTRODUCTION

In 1976, de Gennes coined the nickname *ant in the labyrinth* for the problem of random walks on a fractal structure such as a percolation cluster near the percolation point [1]. In 1982, Wilke *et al.* [2] introduced the *parasite* problem as a variant of the former problem in which a random walk takes place on a lattice animal, i.e., a large percolation cluster in the region right below the percolation point. As far as their universal scaling properties are concerned, lattice animals are closely related to randomly branched polymers (RBPs) in dilute solutions. More precisely: the statistics of swollen lattice animals belongs to the same universality class as RBPs in their swollen phase, and the statistics of collapsing lattice animals belongs to the same universality class as RBPs at the collapse transition ( $\Theta$  line) [3–5]. For both of these distinct universality classes, it is well known that cycles or loops of the animals are irrelevant; i.e., lattice trees also fall into these universality classes. In other words, the lattice animal or RBP on which a random walk takes place in these universality classes is tree-like. Thus, the random walks we study in this paper remind us more of a *monkey on a tree* than a *parasite* on a loop-containing animal, and we prefer to glean our nickname from primatology rather than parasitology.

Topologically, trees are one-dimensional structures. Hence, the backbone between two separated points on a tree consists of a single unique self-avoiding walk (SAW). Therefore, all the scaling dimensions  $d_\alpha$  of the backbone fractals—the backbone itself, the minimal, mean, and maximal paths, the electrical resistance, the red bonds, etc.—are identical:

$$d_B = d_{\min} = d_{\text{SAW}} = d_{\max} = d_R = d_{\text{red}}. \quad (1.1)$$

A clever monkey will climb the minimal path with fractal dimension  $d_{\min}$  to get a coconut at the end of the path. This is in contrast to diffusion, which corresponds to an erratic motion of a monkey. Diffusion, on a fractal medium with

fractal dimension  $d_f$ , is described by the scaling law

$$\langle (\mathbf{r}(t) - \mathbf{r}(0))^2 \rangle = R_N^2 f(t/R_N^{d_w}), \quad (1.2)$$

where  $\mathbf{r}(t)$  is the position of the walker (here, the monkey) at time  $t$ ,  $R_N \sim N^{1/d_f}$  is the gyration radius of the fractal with mass (number of sites)  $N$ , and  $f$  is a scaling function with the properties

$$f(x) \sim \begin{cases} 1 & \text{for } x \rightarrow \infty, \\ x^{2/d_w} & \text{for } x \rightarrow 0. \end{cases} \quad (1.3)$$

As a result of Einstein's relation  $d_w = d_f + d_R$  for the fractal dimension of the random walk, it follows that [6,7]

$$d_w = d_f + d_{\min}. \quad (1.4)$$

As mentioned above, the *monkey on a tree* problem has been around under a different name for some 30 years now. For background, we refer to the review article on diffusion in disordered media by Havlin and Ben-Avraham [7]. In recent years, significant advances have been made in numerical simulations on problems different from but closely related to the monkey on a tree problem. A sophisticated Monte Carlo algorithm has been used to simulate lattice animals and trees in two to nine dimensions [8] and to measure their static scaling exponents with a high precision [9,10]. Furthermore, simulations have been performed to determine with a high precision the fractal and multifractal dimensions of SAWs on percolations clusters in two to four dimensions [11,12]. Hence, we feel that state-of-the-art simulations of diffusion and transport and lattice animals in dimensions suitable for reliable comparison to field theory have become within reach. Thus, we think it is worthwhile to take a fresh look at the monkey on a tree problem with field theoretic methods.

The static fractal dimension  $d_f = 1/\nu_P$  of RBPs or trees are well known [4,5]. Here, we apply renormalized dynamical field theory to calculate  $d_{\min}$  and the related exponents in an  $\varepsilon$  expansion to two-loop order. Since  $d_{\min}$  is equal to the dynamical exponent  $z$ , the scaling exponent of the time a monkey needs to reach a coconut on a tree, we can and will calculate  $d_{\min}$  via calculation of  $z$  of a stochastic process that generates RBPs [5].

\*stenull@physics.upenn.edu

## II. MODEL AND FIELD THEORETIC APPROACH

This section serves two purposes. First, we review the field theoretic model for RBPs that we have developed recently [5]. Some of the steps involved in its derivation are far from trivial, and its symmetry content is rich and interesting. Hence, we think it is worthwhile to review the model in some detail. This will also have the benefit of making the present paper more self-contained. Second, we discuss in broad terms the diagrammatics resulting from our dynamical model for the swollen phase and the collapse transition. We make the observation that the dynamical self-energy diagrams decompose into a quasistatic part and a SAW part that contains all the frequency dependence. This observation is a key to the subsequent sections, as it simplifies the dynamical field theory for the transport and diffusion exponents considerably.

### A. Creation of randomly branched polymers

Our field theoretic model for RBPs is based on the idea of generating their statistics through a mesoscopic stochastic growth process. It is well known that the general epidemic process (GEP) [13] leads to random structures with the properties of percolation clusters [14–17] which are, depending on the parameter values of the GEP, below, at, or above the percolation point. The primary density fields describing this process are the field of agents  $n(\mathbf{r}, t)$  and the field of inactive debris  $m(\mathbf{r}, t) = \lambda \int_{-\infty}^t dt' n(\mathbf{r}, t')$ , which ultimately forms the polymer cluster. The following extension of the GEP is a modification of a process that we have introduced for the description of tricritical isotropic percolation [18]. The non-Markovian Langevin equation describing this process (or, rather, its universality class) is given by

$$\lambda^{-1} \partial_t n = (\nabla^2 + c \nabla m \cdot \nabla) n - \left( r_p + g' m + \frac{f'}{2} m^2 \right) n + \zeta. \quad (2.1)$$

Here, the parameter  $r_p$  tunes the “distance” to the percolation threshold. Below this threshold, in the absorbing phase,  $r_p$  is positive, which we assume throughout this paper. In this case the typical final cluster of the debris generated from a source  $q \delta(\mathbf{r}) \delta(t)$  of agents consists of  $N = \langle \int d^d r m(\mathbf{r}, \infty) \rangle \approx q/r_p$  particles of debris and has a mean diameter (gyration radius)  $\sim 1/\sqrt{r_p}$ . However, here we are not interested in these typical clusters. Rather, we are interested in the large nontypical clusters, the rare events of the stochastic process, with  $N \gg q/r_p$  (in this sense,  $q$  is a small parameter). We know from percolation theory [19] that these clusters belong to the universality class of lattice animals. Hence, they are the same in a statistical sense as RBPs as far as their universal properties go. The gradient term proportional to  $c$  describes the attractive influence of the debris on the agents if  $c$  is negative (as a negative contribution to  $g'$  does). In principle, other gradient terms like  $m \nabla^2 n$  and  $n \nabla^2 m$  could be added to the Langevin equation. However, as long as we have any one of these gradient terms in our theory, an omission of the others has no effect on the final results, and we choose to work with the term proportional to  $c$  only, for simplicity. For usual percolation problems (ordinary or tricritical), all of these gradient terms are irrelevant. As long as  $g' > 0$ , the third-order term  $f' m^2 n$

is irrelevant near the transition point and the process models ordinary percolation near  $r_p = 0$  [15] or nontypical very large clusters, swollen RBPs, for  $r_p > 0$ . We permit both signs of  $g'$  (negative values of  $g'$  correspond to an attraction of the agents by the debris; see above). Hence, our model allows for a tricritical instability (tricritical percolation near  $r_p = 0$  [18] or the collapse transition of the RBPs for  $r_p > 0$  [5]). Consequently we need the third-order term with  $f' > 0$  (representing self-avoidance) to limit the density to finite values in these cases. Physically it originates from the suppression of agents by the debris. The Gaussian noise source  $\zeta(\mathbf{r}, t)$  has correlations

$$\overline{\zeta(\mathbf{r}, t) \zeta(\mathbf{r}', t')} = (\lambda^{-1} g n(\mathbf{r}, t) \delta(t - t') - f n(\mathbf{r}, t) n(\mathbf{r}', t')) \delta(\mathbf{r} - \mathbf{r}'). \quad (2.2)$$

The first part of the noise correlation, Eq. (2.2), takes into account that the agents can decay spontaneously, and thus  $g > 0$ . The term proportional to  $f$  simulates the anticorrelating or correlating (from attraction) behavior of the noise in regions where debris has already been produced. If the coupling constant  $f$  becomes negative, attraction effects prevail. For ordinary percolation this term is irrelevant. The form of the dependence of both parts of the noise correlation on the field is mandated by the fact that the process has to be strongly absorbing in order to model RBPs.

In the past, there have been misconceptions about the relation between absorptivity and the form of the noise correlation, and we think that it is worthwhile to address this relation here in a little more detail. As we just mentioned, our RBP-generating process is, like all percolation processes, strongly absorbing, i.e., its extinction probability [probability that the process becomes extinct in a *finite* time interval  $(0, t)$ ] is larger than 0,  $P_{\text{ext}}(t) > 0$  for  $t < \infty$ . To guarantee this property, all terms in the equation of motion, (2.1), must, of course, contain at least one power of  $n$ . Moreover, and this is the important point here, the expansion of the noise-correlation function, Eq. (2.2), in the density  $n$  must begin with a *linear* term [20]. With respect to enforcing strong absorptivity, a quadratic part in  $n$  of the noise correlation is insufficient. The upshot is that phenomenological considerations are sufficient to uniquely determine the form of the noise. There is no need to resort to a microscopic formulation in terms of master equations or the like to figure out the proper relevant contributions to the noise correlations for the current process, or for percolation processes in general.

### B. Field theoretic functionals

To proceed towards a field theoretic model (for the general method of field theory in statistical physics see, e.g., Refs. [21] and [22]), the Langevin equations, (2.1) and (2.2), are now transformed into a stochastic response functional in the Ito sense [17,23–25],

$$\begin{aligned} \mathcal{J}_{\text{eGEP}}[\tilde{n}, n] = & \int d^d x \left\{ \lambda \int dt \tilde{n} \left( \lambda^{-1} \partial_t - \nabla^2 \right. \right. \\ & \left. \left. - c \nabla m \cdot \nabla + r_p + g' m + \frac{f'}{2} m^2 - \frac{g}{2} \tilde{n} \right) n \right. \\ & \left. + \frac{f}{2} \left( \lambda \int dt \tilde{n} n \right)^2 \right\}, \quad (2.3) \end{aligned}$$

where  $\tilde{n}(\mathbf{r}, t)$  denotes the (imaginary) response field conjugated to  $n(\mathbf{r}, t)$ . With this functional, we now have a vantage point for the calculation of statistical quantities via path integrals with the exponential weight  $\exp(-\mathcal{J}_{\text{eGEP}})$ . When a source term  $(\tilde{j}, \tilde{n})$  is added, where  $\tilde{j}(\mathbf{r}, t) = q\delta(\mathbf{r})\delta(t)$  and  $(\dots, \dots)$  denotes an integral of a product of two fields over space and time, this functional describes, in particular, the statistics of clusters of debris generated by the stochastic growth process, Eq. (2.1), from a source of  $q$  agents at the point  $\mathbf{r} = 0$  at time 0. Denoting by  $\text{Tr}[\dots]$  the functional integration over fields with boundary conditions  $n(\mathbf{r}, -\infty) = \tilde{n}(\mathbf{r}, \infty) = 0$ , we generally have, for the generating functional,

$$\mathcal{Z}[j, \tilde{j}] = \text{Tr}[\exp(-\mathcal{J}_{\text{eGEP}}[\tilde{n}, n] + (\tilde{j}, \tilde{n}) + (j, n))] = 1 \quad (2.4)$$

if the arbitrary source  $j$  or  $\tilde{j}$  is 0. The first property follows from causality, whereas the second one originates from the absorptive properties of the process. Note that the role of causality and adsorptivity can be interchanged by the duality transformation  $m(\mathbf{r}, t) \longleftrightarrow -\tilde{n}(\mathbf{r}, -t)$  [15,17,20].

Averaging an observable  $\mathcal{O}[n]$  over final clusters of debris (RBPs) of a given mass  $N$  generated from the particular source  $\tilde{j}(\mathbf{r}, t) = q\delta(\mathbf{r})\delta(t)$  leads to the quantity [15,17,20]

$$\begin{aligned} \langle \mathcal{O} \rangle_N \mathcal{P}(N) &= \langle \mathcal{O}[n]\delta(N - \mathcal{M}) \exp((\tilde{j}, \tilde{n})) \rangle_{\text{eGEP}} \\ &= \text{Tr}[\mathcal{O}[n]\delta(N - \mathcal{M}) \exp(-\mathcal{J}_{\text{eGEP}} + q\tilde{n}(\mathbf{0}, 0))] \\ &\simeq q \text{Tr}[\mathcal{O}[n]\tilde{n}(\mathbf{0}, 0)\delta(N - \mathcal{M}) \exp(-\mathcal{J}_{\text{eGEP}})], \end{aligned} \quad (2.5)$$

where

$$\mathcal{P}(N) = \langle \delta(N - \mathcal{M}) \exp(q\tilde{n}(\mathbf{0}, 0)) \rangle_{\text{eGEP}} \quad (2.6)$$

is the probability distribution for finding a cluster (an RBP) of mass  $N$ .

$$\mathcal{M} = \int d^d r dt \lambda n(\mathbf{r}, t) = \int d^d r m_\infty(\mathbf{r}) \quad (2.7)$$

is the total mass of the debris. The field  $m_\infty(\mathbf{r}) = m(\mathbf{r}, t = \infty)$  describes the distribution of the debris after the growth process is terminated. Since the probability distribution should be proportional to the number of different configurations, we expect, by virtue of universality arguments, the following proportionality between the probability distribution  $\mathcal{P}(N)$  and the animal number  $\mathcal{A}_N$  for asymptotically large  $N$ :

$$\mathcal{P}(N) \sim N \kappa_0^{-N} \mathcal{A}_N \sim N^{1-\theta} p_0^N, \quad (2.8)$$

where  $\kappa_0$  and  $p_0$  are nonuniversal, in contrast to the universal ‘‘entropic’’ scaling exponent  $\theta$ . The factor  $N$  in Eq. (2.8) arises because the generated clusters are rooted at the source at the point  $\mathbf{r} = 0$ , and each site of a given animal may be the root of a given cluster.

In actual calculations, the  $\delta$  function appearing in averages as in Eqs. (2.5) and (2.6) is hard to handle. This problem can be simplified by using Laplace-transformed observables which are functions of a variable conjugate to  $N$ , say  $z$ , and applying inverse Laplace transformation (where all the singularities of the integrand lie to the left of the integration path) in the end. The switch to Laplace-transformed observables can be done in a pragmatic way by augmenting the original  $\mathcal{J}_{\text{eGEP}}$  with a term  $z\mathcal{M}$  and then working with the new response functional

$$\mathcal{J}_z = \mathcal{J}_{\text{eGEP}} + z\mathcal{M}. \quad (2.9)$$

As an example, let us consider

$$\begin{aligned} \langle \mathcal{O} \rangle_N \mathcal{P}(N) &= \int_{\sigma-i\infty}^{\sigma+i\infty} \frac{dz}{2\pi i} e^{zN} \\ &\times \langle \mathcal{O}[n] \exp(-z\mathcal{M} + q\tilde{n}(\mathbf{0}, 0)) \rangle_{\text{eGEP}}. \end{aligned} \quad (2.10)$$

Note that the relationship between  $\mathcal{P}(N)$  and  $\mathcal{A}_N$  given in Eq. (2.8) signals the existence of a singularity  $\sim (z - z_c)^{\theta-2}$  of the integrand in Eq. (2.10) at some critical value  $z_c$ . Denoting averages with respect to the new functional by  $\langle \dots \rangle_z$ , and defining

$$q\Phi(z) = \ln(\exp(q\tilde{n}))_z \approx q\langle \tilde{n} \rangle_z \quad (2.11)$$

asymptotically, we get, using Jordan’s lemma, that the asymptotic behavior, e.g., of  $\mathcal{P}(N)$  for large  $N$ , is given by

$$\begin{aligned} \mathcal{P}(N) &= \int_{\sigma-i\infty}^{\sigma+i\infty} \frac{dz}{2\pi i} \exp[zN + q\Phi(z)] \\ &\approx q e^{z_c N + q\Phi(z_c)} \int_0^\infty dx \frac{\text{Disc}\Phi(z_c - x)}{2\pi i} e^{-xN}, \end{aligned} \quad (2.12)$$

where the last row gives the asymptotics for large  $N$ . Here,  $z_c$  is the first singularity of  $\Phi(z) \sim (z - z_c)^{\theta-2}$ , which is a branch point on the negative real axis, and the contour of the path integral is deformed into a path above and below the branch cut beginning at the singularity.  $\text{Disc}\Phi$  denotes the discontinuity of the function  $\Phi$  at the branch cut. The nonuniversal factor  $q e^{z_c N + q\Phi(z_c)}$  depending exponentially on  $N$  is common to all averages defined by Eq. (2.5) and therefore cancels from all mean values  $\langle \mathcal{O} \rangle_N$ .

Now we return to our response functional  $\mathcal{J}_z$  to refine it into a form that suits us best for our actual field theoretic analysis. As discussed above, the gradient term proportional to  $c$  is redundant. To eliminate this term, we apply to the field  $\tilde{n}$  the shift and mixing transformation

$$\tilde{n}(\mathbf{r}, t) \rightarrow \tilde{n}(\mathbf{r}, t) + a - acm_\infty(\mathbf{r}), \quad (2.13)$$

where  $a$  is a free parameter at this stage. Ultimately, this parameter is defined by  $\langle \tilde{n} \rangle = 0$ , which means that the diagrammatic perturbation expansion is free of tadpoles. Defining  $\tau = r_p - ga$ ,  $\rho = (g' + fa)a - ac\tau$ , and  $h = z + r_p a - ga^2/2$ , the stochastic functional  $\mathcal{J}_z$ , Eq. (2.9), takes the form

$$\begin{aligned} \mathcal{J}_z &= \int d^d x \left\{ \lambda \int dt \tilde{n} \left( \lambda^{-1} \partial_t + \tau - \nabla^2 + g'_2 m - \frac{g_2}{2} \tilde{n} \right. \right. \\ &\left. \left. + g_1 m_\infty \right) n + \left( \frac{\rho}{2} m_\infty^2 + \frac{g_0}{6} m_\infty^3 + h m_\infty \right) \right\}. \end{aligned} \quad (2.14)$$

Here, we could have set  $\tau$  equal to 0 by exploiting that  $a$  is a free parameter. Instead of doing so, we keep  $\tau$  in our theory as a small, free, redundant parameter. We see later on that keeping  $\tau$  comes in handy for renormalization purposes. In Eq. (2.14), we have eliminated couplings that are of more than third order in the fields because they are irrelevant. We do not write down in detail the relatively uninteresting relations between the new third-order coupling constants and the old ones. Note that  $\mathcal{J}_z$  contains two similar couplings:  $g'_2 \tilde{n} n m$  and  $g_1 \tilde{n} n m_\infty$ . Whereas the first coupling respects causal ordering, which means that  $\tilde{n}$  is separated by an infinitesimal positive time element from the  $n m$  part resulting from the Ito calculus [25], the second

one respects causality only between  $\tilde{n}$  and  $n$ . In contrast to the  $m$  part, the  $m_\infty$  part contains all the  $n$  with times that lie in the past and in the future of  $\tilde{n}$ . This property is the heritage of the time-delocalized noise term and of the introduction of the  $\delta$  function in Eq. (2.5) as a final ( $t = \infty$ ) condition that destroyed the causality of  $\mathcal{J}_z$ . Even if we had disregarded the noise term proportional to  $f$  in Eq. (2.2) initially, the  $\tilde{n}nm_\infty$  coupling would be generated by coarse graining, and hence it must be ultimately incorporated into the theory to yield renormalizability.

The relevance or irrelevance of the different terms in  $\mathcal{J}_z$  follows from their dimensions with respect to an inverse length scale  $\mu$  such that time scales as  $\mu^{-2}$ . Fundamentally, one has to decide which parameters are the critical control parameters going to 0 in mean-field theory. At the collapse transition these are  $\tau \sim \rho \sim \mu^2$  and  $h \sim \mu^{(d+2)/2}$  [5]. The dimensions of the fields are then given by  $\tilde{n} \sim m \sim \mu^{(d-2)/2}$  and  $n \sim \mu^{(d+2)/2}$ . It follows that all the coupling constants  $g_0, g_1, g_2$ , and  $g'_2$  have the same dimension  $\mu^{(6-d)/2}$ . Note that  $\tilde{n}$  is always tied to at least one factor of  $n$  as a result of the absorptivity of the process. Hence, all the terms in  $\mathcal{J}_z$  are relevant for  $d \leq 6$  spatial dimensions, and the upper critical dimension of the collapse transition is  $d_c = 6$ . The situation is different if  $\rho$  is a finite positive quantity that is in the swollen phase. Then  $\rho$  can be absorbed into the fields by a rescaling transformation which amounts to formally setting  $\rho = 2$ . The field dimensions then become  $m \sim \mu^{d/2}, n \sim \mu^{(d+4)/2}$ , and  $\tilde{n} \sim \mu^{(d-4)/2}$ . It follows that  $h \sim \mu^{d/2}, g_0 \sim \mu^{-d/2}, g_1 \sim \mu^{(4-d)/2}, g'_2 \sim \mu^{(2-d)/2}$ , and  $g_2 \sim \mu^{(8-d)/2}$ . Hence, in the swollen phase, only  $g_2 = g$  is relevant, now below eight spatial dimensions. The other couplings can be safely removed. Then  $\mathcal{J}_z$  reduces to the dynamical response functional of the usual simple GEP.

Recently, we have shown that  $g'_2$  becomes weakly irrelevant [with a correction exponent of order  $O(6-d)$ ] at the renormalization-group (RG) fixed point corresponding to the collapse transition of RBPs [5]. Hence, we can neglect this coupling not only for the swollen phase but also for the collapse transition, even though dimensional analysis suggests its relevance for the latter in the vicinity of the Gaussian fixed point. In Ref. [5] we argued that the vanishing of  $g'_2$  indicates that cycles or loops of RBPs are irrelevant. In other words, large RBPs in the swollen phase and at the collapse transition are dominated by tree configurations.

The last step in setting up the response functional for the dynamical description of swollen or collapsing RBPs is a duality transformation that interchanges absorptivity in favor of causality:

$$\begin{aligned} \tilde{n}(\mathbf{r}, t) &= s(\mathbf{r}, -t), & n(\mathbf{r}, t) &= \tilde{s}(\mathbf{r}, -t), \\ m(\mathbf{r}, t) &= \lambda \int_{-t}^{\infty} dt' \tilde{s}(\mathbf{r}, t'), \\ m_\infty(\mathbf{r}) &= m(\mathbf{r}, \infty) =: \tilde{\varphi}(\mathbf{r}). \end{aligned} \tag{2.15}$$

This step leads to the response functional

$$\begin{aligned} \mathcal{J} &= \int d^d x \left\{ \lambda \int dt \tilde{s} \left( \lambda^{-1} \partial_t + \tau - \nabla^2 + g_1 \tilde{\varphi} - \frac{g_2}{2} s \right) s \right. \\ &\quad \left. + \left( \frac{\rho}{2} \tilde{\varphi}^2 + \frac{g_0}{6} \tilde{\varphi}^3 + h \tilde{\varphi} \right) \right\}, \end{aligned} \tag{2.16}$$

which serves us in the following as the vantage point of our dynamical field theory.

In this paper, we are mainly interested in the dynamical aspects of our theory. On occasion, however, we also discuss some of its static aspects. On one hand, this will make our presentation more self-contained because we will need some of the previously derived static results as input as we move along. On the other hand, we feel that certain elements of the theory are more easily discussed statically rather than dynamically. For the static aspects, we do not need the full response functional. Rather it is sufficient to consider the quasistatic Hamiltonian

$$\begin{aligned} \mathcal{H} &= \int d^d x \left\{ \tilde{\varphi}(\tau - \nabla^2)\varphi + \frac{\rho}{2} \tilde{\varphi}^2 + h \tilde{\varphi} \right. \\ &\quad \left. + \frac{g_0}{6} \tilde{\varphi}^3 + g_1 \tilde{\varphi}^2 \varphi - \frac{g_2}{2} \tilde{\varphi} \varphi^2 \right. \\ &\quad \left. + \bar{\psi}(\tau - \nabla^2 + g_1 \tilde{\varphi} - g_2 \varphi)\psi \right\}, \end{aligned} \tag{2.17}$$

which follows from  $\mathcal{J}$  by setting  $s(\mathbf{r}, t) \rightarrow \varphi(\mathbf{r})$ . Here, we have added a pair of fermionic ghost fields  $(\bar{\psi}, \psi)$  that automatically guarantees the original causality rule in Feynman diagrams through its couplings to the fields  $\tilde{\varphi}$  and  $\varphi$  [5]. We note that the quasistatic Hamiltonian has Becchi-Rouet-Stora (BRS) supersymmetry, which indicates that only tree-like polymer configurations are relevant as noted above.

### C. Diagrammatics: SAWs on tree diagrams

Figure 1 shows the diagrammatic elements of our theory as resulting from  $\mathcal{J}$  and  $\mathcal{H}$ . There is the dynamic propagator, which reads

$$G(\mathbf{q}, t) = \theta(t) \exp[-(\tau + \mathbf{q}^2)t] \tag{2.18}$$

in momentum-time representation or, after Fourier transformation,

$$\tilde{G}(\mathbf{q}, \omega) = \frac{1}{i\lambda\omega + \tau + \mathbf{q}^2} \tag{2.19}$$

in momentum-frequency representation. Its static counterpart is given by

$$C(\mathbf{q}) = \tilde{G}(\mathbf{q}, 0) = \frac{1}{\tau + \mathbf{q}^2}. \tag{2.20}$$

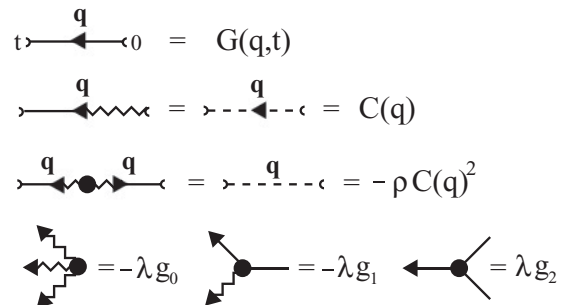


FIG. 1. Elements of the dynamic Feynman diagrams.

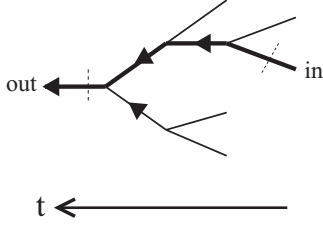


FIG. 2. A tree-like subdiagram.

The dynamical functional also features the static correlator

$$-\rho C(\mathbf{q})^2 = \frac{-\rho}{(\tau + \mathbf{q}^2)^2}. \quad (2.21)$$

Note the negative sign of the correlator, which has its origin in the fact that the fluctuations of the fields  $s$  and  $\varphi$  are purely imaginary (a heritage of the imaginary response field  $\tilde{n}$ ). In addition to these elements represented by lines, there are the three vertices shown at the bottom of Fig. 1.

Recall that we are primarily interested in scaling exponents for transport and diffusion on RBPs. These we extract from the response function

$$G_{1,1}(\mathbf{r}, t) = \langle n(\mathbf{r}, t) \tilde{n}(\mathbf{0}, 0) \rangle = \langle s(-\mathbf{r}, t) \tilde{s}(\mathbf{0}, 0) \rangle \quad (2.22)$$

and its renormalizations. Its (quasi-)static renormalizations are well known from earlier work [4,5,29]. Its dynamical renormalization is known only to one-loop order for the swollen phase, as shown by one of us [15], and is entirely unknown for the collapse transition. Hence, it is our main task here to calculate the renormalization factor  $Z_\lambda$  pertaining to the dynamical coefficient  $\lambda$ . To this end, we consider the one-particle irreducible amputated self-energy diagrams with an outgoing amputated  $\tilde{s}$  leg and an ingoing amputated  $s$  leg. Let us forget for the moment all the static  $C$  lines in a diagram that are introduced by the couplings to the static field  $\tilde{\varphi}$ . Then any of these diagrams is reduced to a pure time-ordered tree diagram that has its origin in the outgoing amputated  $\tilde{s}$  leg (see Fig. 2). The tree consists of  $G$  lines and  $g_2$  vertices. The ingoing amputated  $s$  leg is one of the pending  $s$  legs. The SAW along  $G$  lines which connects the two amputated legs is unique. Note that the tree structure with this unique SAW is a consequence of the limit  $g_2' \rightarrow 0$ , which we may hence call the tree limit. Now we reintroduce the  $C$  lines by inserting  $g_0$ ,  $g_1$ , and  $\rho$  vertices and saturating the pending nonamputated  $s$  legs with the static  $\tilde{\varphi}$  legs. Then, integrating over internal times from right (earlier times) to left (later times), it is easy to see that the internal  $\tilde{s}$  legs are converted by the integrations into  $\tilde{\varphi}$  legs with the exception of the  $\tilde{s}$ 's that are part of the connecting SAW between the two amputated external legs. The conversion of  $\tilde{s}$  legs into  $\tilde{\varphi}$  legs turns the corresponding  $G$  lines into  $C$  lines. In other words, the parts of the diagram that do not belong to the connecting SAW become purely quasistatic. One can think of the time integrations as having the net effect of decomposing any self-energy diagram into a dynamic part, the connecting SAW, and a quasistatic residual part. This decomposition is visualized in Fig. 3. After the decomposition, the frequency dependence of any self-energy diagrams resides solely in its connecting SAW. To calculate the dynamical renormalization factor  $Z_\lambda$ , we have to calculate the parts of the self-energy diagrams that are proportional

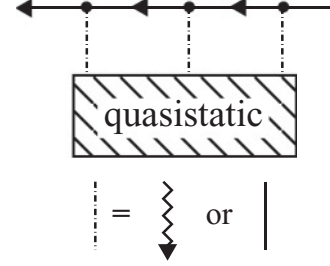


FIG. 3. Decomposition of a self-energy diagram into a dynamic part, the connecting SAW, and a quasi-static part.

to  $i\omega$ , which we can do, following standard field theoretic procedures, by making  $i\omega s \tilde{s}$  insertions. After what we have just learned about the decomposition effect of the time integrations, it is clear that we need to put these insertions only into the  $G$  lines forming the connecting SAW.

All these considerations are easily generalized from self-energy diagrams to a general one-particle irreducible diagram with  $\tilde{N}$  external  $\tilde{s}$  legs and  $N$  external  $s$  legs. Let us consider such a diagram beginning, as above, by temporarily omitting all static  $C$  lines. This leads to a decomposition of the diagram into a (spanning) forest of  $\tilde{N}$  disconnected time-directed trees rooted in the outgoing amputated  $\tilde{s}$  legs, each featuring a subset of the  $N$  incoming amputated  $s$  legs. Then Fourier transformation from time arguments to frequencies shows that the frequency flowing out through an  $\tilde{s}$  leg is the sum of the frequencies flowing into the diagram through the corresponding set of  $s$  legs. Thus, there are  $\tilde{N}$  frequency-conservation laws. The argument concludes by tying together the disconnected trees by readmitting the static  $C$  lines.

### III. THE SWOLLEN RANDOMLY BRANCHED POLYMER

In this section, we use our model and our insight into the structure of the diagrammatic expansion developed in Sec. II C to calculate the dynamical exponent  $z$  and the related transport exponents for the swollen phase. Before we embark on this quest, we briefly review some of the quasistatic results that we can utilize as input for our dynamical calculation. Furthermore, we have performed rational approximations to improve the known results for the static exponents that we present here, along with comparisons to the available numerical results for these exponents.

#### A. Functionals, renormalizations, and static results

As discussed above,  $g_0$ ,  $g_1$ , and  $g_2'$  are strongly irrelevant for the swollen phase, and hence we now set  $g_0 = g_1 = g_2' = 0$ . Moreover,  $\rho$  is a finite and positive quantity that can be reset through a simple rescaling transformation. Hence, we have the freedom to choose  $\rho = 2$  for simplicity, and we do so. With these settings, the response functional reduces to

$$\mathcal{J}_{sw} = \int d^d x \left\{ \lambda \int dt \tilde{s} \left( \lambda^{-1} \partial_t + \tau - \nabla^2 - \frac{g}{2} s \right) s + (\tilde{\varphi}^2 + h\tilde{\varphi}) \right\}, \quad (3.1)$$

where  $g = g_2$ . This functional describes, besides the dynamical creation of the swollen RBPs, the dynamics at the Yang-Lee singularity [26], however, with quenched static noise [15]. With the settings for the swollen phase, the quasistatic Hamiltonian including ghost fields becomes

$$\begin{aligned} \mathcal{H}_{sw} &= \int d^d x \left\{ \tilde{\varphi} \left( \tau - \nabla^2 - \frac{g}{2} \varphi \right) \varphi + \tilde{\varphi}^2 + h \tilde{\varphi} \right. \\ &\quad \left. + \tilde{\psi} (\tau - \nabla^2 - g \varphi) \psi \right\} \\ &= \int d^d x d\theta d\bar{\theta} \left\{ \frac{1}{2} \Phi (\tau - \square) \Phi - \frac{g}{6} \Phi^3 + h \Phi \right\}, \end{aligned} \quad (3.2)$$

where we have introduced Grassmannian anticommuting supercoordinates  $\theta$  and  $\bar{\theta}$ , with integration rules  $\int d\theta 1 = 0$ ,  $\int d\bar{\theta} 1 = 0$ ,  $\int d\theta \theta = 1$ ,  $\int d\bar{\theta} \bar{\theta} = 1$ , and defined a superfield  $\Phi(\mathbf{r}, \bar{\theta}, \theta) = \varphi(\mathbf{r}) + i\bar{\theta}\psi(\mathbf{r}) + i\tilde{\psi}(\mathbf{r})\theta + \bar{\theta}\tilde{\varphi}(\mathbf{r})$ , as well as the super-Laplace operator  $\square = \nabla^2 + 2\partial_{\bar{\theta}}\partial_{\theta}$ . The Hamiltonian  $\mathcal{H}_{sw}$  shows full supersymmetry, i.e., besides the symmetry against supertranslations (BRS symmetry), it also has super-rotation symmetry. Parisi and Sourlas [4] showed some 30 years ago that the full supersymmetry leads to dimensional reduction because it makes the Hamiltonian equivalent to the ordinary Yang-Lee-Hamiltonian in two lesser dimensions (see also the rigorous work on the dimensional reduction by Brydges and Imbrie [27,28]). Exploiting this relation, all static renormalizations are known up to third order [29].

We note that, in contrast to the quasistatic Hamiltonian, which, as we just have seen, can be written in the form of the supersymmetric Yang-Lee Hamiltonian by the introduction of a superfield, the dynamic response functional is not supersymmetric. Hence, we unfortunately cannot exploit dimensional reduction in our dynamic calculation.

In the following, we use dimensional regularization. For the swollen phase, we employ the renormalization scheme

$$s \rightarrow \hat{s} = Z^{1/2}s, \quad \tilde{s} \rightarrow \hat{\tilde{s}} = Z_{\lambda} Z^{1/2}\tilde{s}, \quad (3.3a)$$

$$\lambda \rightarrow \hat{\lambda} = Z_{\lambda}^{-1}\lambda, \quad \tau \rightarrow \hat{\tau} = Z^{-1}Z_{\tau}\tau, \quad (3.3b)$$

$$g \rightarrow \hat{g} = Z^{-3/2}Z_g g, \quad G_{\varepsilon} g^2 = u\mu^{\varepsilon}, \quad (3.3c)$$

$$h \rightarrow \hat{h} = Z^{-1/2} \left( h - \frac{g}{2} A \tau^2 \right), \quad (3.3d)$$

$$(\tilde{\varphi}, \varphi, \tilde{\psi}, \psi) \rightarrow (\hat{\tilde{\varphi}}, \hat{\varphi}, \hat{\tilde{\psi}}, \hat{\psi}) = Z^{1/2}(\tilde{\varphi}, \varphi, \tilde{\psi}, \psi). \quad (3.3e)$$

Not all the renormalization  $Z$  factors in the renormalization scheme are independent. The form invariance of  $\mathcal{J}_{sw}$  and  $\mathcal{H}_{sw}$  under the shift  $s \rightarrow s + \alpha$  leads to the Ward identities  $Z_g = Z_{\tau}$  and  $Z_{\tau} = 1 + g^2 A$  [26]. As mentioned above, the  $Z$  factors other than  $Z_{\lambda}$  are known to three-loop order. In our dynamical two-loop calculation, we exploit the known result for the field renormalization  $Z$  to two-loop order as an input,

$$Z = 1 + \frac{u}{3\varepsilon} + \left( 5 - \frac{13}{12}\varepsilon \right) \left( \frac{u}{3\varepsilon} \right)^2 + O(u^3), \quad (3.4)$$

where  $\varepsilon = 8 - d$ .

For completeness, let us mention here that the known three-loop result for the entropic scaling exponent  $\theta$  as featured in Eq. (2.8) reads [29]

$$\theta = \frac{5}{2} - \frac{\varepsilon}{12} - \frac{79}{3888}\varepsilon^2 + \left( \frac{\zeta(3)}{81} - \frac{10445}{1259712} \right) \varepsilon^3 + O(\varepsilon^4). \quad (3.5)$$

The scaling exponent  $\nu_p$  of the gyration radius of the branched polymer,  $R_N \sim N^{\nu_p}$ , is related to  $\theta$  by

$$\theta = (d - 2)\nu_p + 1. \quad (3.6)$$

The resulting  $\varepsilon$  expansion of  $\nu_p$  reads

$$\begin{aligned} \nu_p &= \frac{1}{4} + \frac{\varepsilon}{36} + \frac{29}{23328}\varepsilon^2 \\ &\quad + \left( \frac{\zeta(3)}{486} - \frac{8879}{7558272} \right) \varepsilon^3 + O(\varepsilon^4). \end{aligned} \quad (3.7)$$

Now we improve these results by making rational approximations that incorporate the exact results that are known for  $\theta$  in dimensions  $d$  from 1 to 4, namely,  $\theta(d=1) = 0$ ,  $\theta(d=2) = 1$ ,  $\theta(d=3) = 3/2$ , and  $\theta(d=4) = 11/6$ . We get

$$\theta \approx \frac{5}{2} - \frac{\varepsilon}{12} \left( \frac{1 + 1.37622\varepsilon - 0.0130833\varepsilon^2 - 0.0171653\varepsilon^3}{1 + 1.13239\varepsilon - 0.210607\varepsilon^2 + 0.00685362\varepsilon^3} \right). \quad (3.8)$$

For  $\nu_p$ , we include the exact values  $\nu_p(d=1) = 1$ ,  $\nu_p(d=3) = 1/2$ , and  $\nu_p(d=4) = 5/12$  and get

$$\nu_p \approx \frac{1}{4} + \frac{\varepsilon}{36} \left( \frac{1 + 1.17714\varepsilon - 0.113178\varepsilon^2}{1 + 1.13239\varepsilon - 0.210607\varepsilon^2 + 0.00685362\varepsilon^3} \right). \quad (3.9)$$

With regard to relation (3.6), we note that our independent rational approximations satisfy these relations to order  $O(10^{-6})$ . In Table I, we compare the numerical values resulting from these approximations for various dimensions to recent simulation results of Hsu, Nadler, and Grassberger [9,10]. Overall, the two agree remarkably well over a wide range of dimensions.

### B. Calculation of the dynamical scaling exponent

Now we return to our main goal, the two-loop calculation of the dynamical exponent  $z$  via the calculation of  $Z_{\lambda}$ . As a warmup, let us first do a quick one-loop calculation that reproduces the known one-loop result. At this order, there is only one self-energy diagram, namely, diagram (1) in Fig. (4). Using the graphical elements pictured in Fig. 1, this diagram

TABLE I. Rational-approximation estimates of the exponents  $\theta$  and  $\nu_p$  compared with simulation results of Hsu, Nadler, and Grassberger [9].

$d$	1	2	3	4	5	6	7	8
$\theta$	0	1	3/2	11/6	2.0769	2.2603	2.3986	5/2
Hsu <i>et al.</i>				1.835(6)	2.080(7)	2.261(12)	2.40(2)	
$\nu_p$	1	0.64267	1/2	5/12	0.35896	0.31507	0.27973	1/4
Hsu <i>et al.</i>		0.6412(5)		0.4163(30)	0.359(4)	0.315(4)	0.282(5)	

translates into the formula

$$(1) = \lambda g^2 \int_{\mathbf{p}} \frac{(-2)}{(\tau + \mathbf{p}^2)^2 (i\omega/\lambda + \tau + (\mathbf{p} - \mathbf{q})^2)}, \quad (3.10)$$

where  $\int_{\mathbf{p}} \dots$  is an abbreviation for the  $d$ -dimensional momentum integral  $(2\pi)^{-d} \int d^d p \dots$ . The calculation of this and, in particular, that of the higher order diagrams can be simplified by resorting to massless propagators. Practically, this is done by expanding the integrands in powers of  $i\omega/\lambda$  and  $\tau$ . For the one-loop diagram (1) in Fig. 4, this gives

$$(1) = -2\lambda g^2 \int_{\mathbf{p}} \left\{ \frac{1}{(\mathbf{p} - \mathbf{q})^2 (\mathbf{p}^2)^2} - \frac{i\omega/\lambda + \tau}{((\mathbf{p} - \mathbf{q})^2)^2 (\mathbf{p}^2)^2} - \frac{2\tau}{(\mathbf{p} - \mathbf{q})^2 (\mathbf{p}^2)^3} + \dots \right\}. \quad (3.11)$$

Note that the massless integrals produced by the expansion are not IR divergent as long as  $d > 6$ . For the calculation of these integrals, we refer to Appendix A. Their  $\varepsilon$  expansions about  $d = 8$  lead to the renormalized vertex function to one-loop order:

$$\Gamma_{1,1}^{(1L)}(q, \omega) = (ZZ_\lambda i\omega + Z_\tau \lambda \tau + Z\lambda q^2) - \frac{u}{3\varepsilon} (2i\omega + 6\lambda \tau + \lambda q^2) + \dots \quad (3.12)$$

Hence, we obtain to this order

$$Z = Z_\lambda = 1 + \frac{u}{3\varepsilon}, \quad Z_\tau = 1 + \frac{2u}{\varepsilon}, \quad (3.13)$$

which leads to the one-loop result  $z = 2 + \eta + O(\varepsilon^2)$  [15], where  $\eta = -\varepsilon/9 + O(\varepsilon^2)$  is the anomalous dimension of field  $s$  [26].

Now turn to the two-loop part of the calculation, for which we consider the two-loop diagrams in Fig. 1. The parts of these

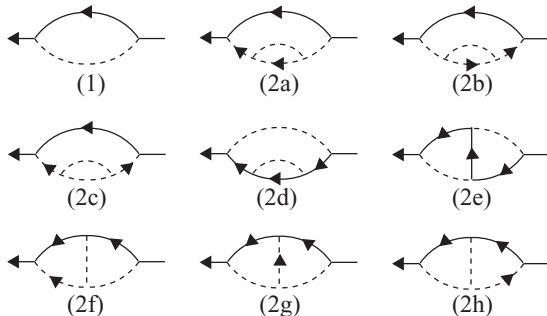


FIG. 4. Self-energy diagrams for swollen RBPs to two-loop order.

diagrams linear in  $i\omega$  are

$$((2a) + (2b) + (2c))_{i\omega} = (2F(5,2,1) + \frac{1}{2}F(4,2,2))(-4i\omega g^4), \quad (3.14a)$$

$$(2d)_{i\omega} = (2F(5,2,1) + F(4,2,2))(-4i\omega g^4), \quad (3.14b)$$

$$(2e)_{i\omega} = (2F(4,3,1) + F(3,3,2))(-4i\omega g^4), \quad (3.14c)$$

$$((2f) + (2g) + (2h))_{i\omega} = (2F(4,3,1) + 2F(4,2,2) + 2F(3,3,2))(-4i\omega g^4), \quad (3.14d)$$

where the  $F(\dots)$  are the frames of the diagrams, i.e., their parts consisting only of the momentum integrations, without any coupling constants or symmetry factors. For a more precise definition of the  $F(\dots)$ , we refer to Appendix A. Next, we calculate the counter-terms of these frames. For simplicity of the argument, let us just say here that we apply some calculation procedure  $\mathfrak{C}$  to the frames that produces as its result the counter-terms of the frames:

$$\mathfrak{C} F(\dots) = C(\dots). \quad (3.15)$$

A precise definition of  $\mathfrak{C}$ , along with some details of the calculations, is given in Appendix A. Application of  $\mathfrak{C}$  results in

$$\begin{aligned} \mathfrak{C}((2a) + \dots + (2h))_{i\omega} &= \left( 4C(5,2,1) + \frac{7}{2}C(4,2,2) + 4C(4,3,1) \right. \\ &\quad \left. + 3C(3,3,2) \right) (-4i\omega g^4) = \frac{11}{9\varepsilon^2} \left( 1 - \frac{43}{132}\varepsilon \right) i\omega u^2. \end{aligned} \quad (3.16)$$

These counter-terms yield the two-loop contribution to the renormalization-factor product

$$ZZ_\lambda = 1 + \frac{2u}{3\varepsilon} + \frac{11}{9\varepsilon^2} \left( 1 - \frac{43}{132}\varepsilon \right) u^2 + O(u^3). \quad (3.17)$$

Using Eq. (3.4), we finally obtain the wanted dynamic renormalization factor:

$$Z_\lambda = 1 + \frac{u}{3\varepsilon} + \frac{5}{9\varepsilon^2} \left( 1 - \frac{\varepsilon}{2} \right) u^2 + O(u^3). \quad (3.18)$$

Next, we discuss the RG equation (RGE) for the vertex functions and its solution. As the result of the dynamic tree structure in the Feynman diagrams, the vertex functions  $\Gamma_{\tilde{N},N}(\{\omega/\lambda\}, \{\mathbf{q}\}, \tau, u, \mu)$  depend only on the incoming frequencies of the  $N$   $s$  legs. Setting these frequencies to 0, we get, in

TABLE II. Rational-approximation estimates of the fractal dimensions of swollen RBPs compared with numerical results of Havlin *et al.* [6].

$d$	1	2	3	4	5	6	7	8
$d_w$	2	2.7138	3.3127	3.8638	4.3960	4.9238	5.4560	6
Havlin <i>et al.</i>		2.78(8)	3.37(10)	3.89(12)				
$d_{\min}$	1	1.1578	1.3127	1.4638	1.6101	1.7499	1.8811	2
Havlin <i>et al.</i>		1.17(8)	1.36(10)	1.49(12)				
$d_f$	1	1.5560	2	12/5	2.7859	3.1739	3.5749	4

the case  $\tilde{N} = 1$ , the static vertex functions

$$\Gamma_{1,N}^{(\text{stat})}(\{\mathbf{q}\}) = \Gamma_{1,N}(\{\omega/\lambda = 0\}, \{\mathbf{q}\}), \quad (3.19)$$

which are related by dimensional reduction to the vertex functions  $\Gamma_{N+1}^{(YL)}$  of the Yang-Lee theory in two lesser dimensions. The RGE of the dynamical  $\Gamma_{\tilde{N},N}$  reads [26]

$$\mathcal{D}_\mu \Gamma_{\tilde{N},N} = \gamma \frac{(\tilde{N} + N)}{2} \Gamma_{\tilde{N},N} - \gamma_\tau \frac{\tau^2}{2g} \delta_{\tilde{N},1} \delta_{N,0}, \quad (3.20)$$

where

$$\mathcal{D}_\mu = \mu \partial_\mu + \zeta \lambda \partial_\lambda + \beta \partial_u + \kappa \tau \partial_\tau \quad (3.21)$$

is the RG differential operator, and

$$\begin{aligned} \gamma &= \mu \partial_\mu \ln Z|_0, & \gamma_\tau &= \mu \partial_\mu \ln Z_\tau|_0, & \zeta &= \mu \partial_\mu \ln Z_\lambda|_0, \\ \kappa &= \gamma - \gamma_\tau, & \beta &= (-\varepsilon + 3\gamma - 2\gamma_\tau)u. \end{aligned} \quad (3.22)$$

For the Wilson functions featured here, we have the expansions

$$\begin{aligned} \gamma &= -\frac{u}{3} + \frac{13}{54}u^2 + O(u^3), & \gamma_\tau &= -2u + \frac{23}{6}u^2 + O(u^3), \\ \zeta &= -\frac{u}{3} + \frac{5}{9}u^2 + O(u^3). \end{aligned} \quad (3.23)$$

The fixed point  $u_*$  of the RGE determined by  $\beta(u_*) = 0$  reads

$$u_* = \frac{\varepsilon}{3} + \frac{125}{486}\varepsilon^2 + O(\varepsilon^3). \quad (3.24)$$

At this fixed point, it follows that

$$\varepsilon - 2\kappa(u_*) = \gamma(u_*) = \eta. \quad (3.25)$$

Hence, the static exponent  $\eta$  and the dynamic exponent

$$z = 2 + \zeta(u_*) \quad (3.26)$$

are the only independent critical exponents of the problem.

Shift-invariant observables free of redundancies are

$$M = \tau - g(s), \quad H = 2gh + \tau^2, \quad (3.27)$$

with RGEs

$$\mathcal{D}_\mu M = \kappa M, \quad \mathcal{D}_\mu H = (\gamma + \kappa)H. \quad (3.28)$$

Note that  $M$  and  $H$  are linearly related to the Laplace transform  $\Phi(z)$  of the cluster probability  $\mathcal{P}(N)$  and the original Laplace variable  $z$ , respectively.  $M$  replaces the redundant parameter  $\tau$  in all shift-invariant quantities. The integration of the RGEs, Eqs. (3.28), at the fixed point yields the equation of state [26],

$$M = \text{const } H^{\theta-2}. \quad (3.29)$$

Likewise, by integrating the RGE, (3.20), at the fixed point, we obtain

$$\langle s(\mathbf{r}, t) \tilde{s}(\mathbf{0}, 0) \rangle = \frac{F(t/r^z, r H^{\nu_p})}{r^{d-2+\eta+z}} \quad (3.30)$$

for the response function. The static exponents are related by

$$\nu_p = \frac{2}{d-\eta}, \quad \theta - 2 = \frac{d-4+\eta}{d-\eta}, \quad (3.31)$$

in conformity with relation (3.6). For the dynamical exponent, we obtain the two-loop result

$$z = 2 + \zeta(u_*) = 2 - \frac{\varepsilon}{9} - \frac{35}{18} \left( \frac{\varepsilon}{9} \right)^2 + O(\varepsilon^3). \quad (3.32)$$

Finally, we improve the numerical accuracy of this result by incorporating the exact value  $z = 1$  for  $d = 1$  ( $\varepsilon = 7$ ) through the rational approximation

$$d_{\min} = z \approx 2 - \varepsilon \frac{1134 + 245\varepsilon}{10206 + 1391\varepsilon}. \quad (3.33)$$

Using relation (1.4) together with  $d_f = 1/\nu_p$  and in conjunction with the rational approximations given in Eqs. (3.9) and (3.33), we obtain the fractal dimensions displayed in Table II and Figs. 5 and 6. These figures also show the available simulation results [6]. We find that our field theoretical results agree remarkably well with the latter.

For completeness, we would like to mention that Gould and Kohin [30] calculated  $d_w$  for two dimensions almost 30 years ago using the real-space RG. Their result,  $d_w = 2.18$ , is about 20% lower than the corresponding values in Table II.

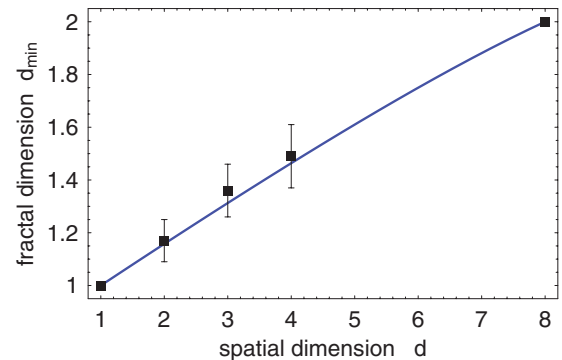


FIG. 5. (Color online) Rational-approximation estimate of the fractal dimension of the minimal path compared with numerical results of Ref. [6].

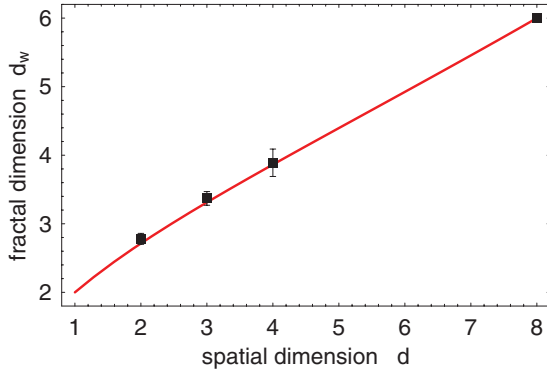


FIG. 6. (Color online) Rational-approximation estimate of the fractal dimension of the random walk compared with numerical results of Ref. [6].

#### IV. THE COLLAPSING RANDOMLY BRANCHED POLYMER

Now we turn to the collapse transition. As we did for the swollen phase, we first briefly review some known results [5] that we need as input as we move along. The main task is, once again, the calculation of the dynamical exponent  $z$  via the calculation of the dynamical renormalization  $Z_\lambda$ .

##### A. Static renormalizations and results

As discussed in Sec. II,  $g_0$ ,  $g_1$ , and  $g_2$  are all relevant for the collapse transition and hence need to be kept in the field theoretic functionals. As also discussed,  $g'_2$  is weakly irrelevant at the collapse transition, and hence we can take the tree limit  $g'_2 \rightarrow 0$  here. Thus, we work with the response functional  $\mathcal{J}$  as given in Eq. (2.16) and, as far as the static properties are concerned, the quasistatic Hamiltonian  $\mathcal{H}$  as given in Eq. (2.17).

Our renormalization scheme for the latter in dimensional regularization is

$$(\tilde{\varphi}, \varphi, \tilde{\psi}, \psi) \rightarrow (\hat{\varphi}, \hat{\varphi}, \hat{\psi}, \hat{\psi}) = Z^{1/2}(\tilde{\varphi}, \varphi + K\tilde{\varphi}, \tilde{\psi}, \psi), \quad (4.1a)$$

$$\underline{\tau} \rightarrow \hat{\underline{\tau}} = Z^{-1} \underline{Z} \cdot \underline{\tau}, \quad (4.1b)$$

$$h \rightarrow \hat{h} = Z^{-1/2} \left( h + \frac{1}{2} G_\varepsilon^{1/2} \mu^{-\varepsilon/2} \underline{\tau} \cdot \underline{A} \cdot \underline{\tau} \right), \quad (4.1c)$$

$$G_\varepsilon^{1/2} g_\alpha \rightarrow G_\varepsilon^{1/2} \hat{g}_\alpha = Z^{-3/2} (u_\alpha + B_\alpha) \mu^{\varepsilon/2}, \quad (4.1d)$$

where  $\underline{\tau} = (\rho, \tau)$  and where  $\varepsilon$  now measures the deviation from  $d = 6$ ,  $\varepsilon = 6 - d$ . Since we are not interested here in the renormalization of the control parameter  $\rho$  that defines the crossover variable to the swollen phase and that goes to 0 at the collapse or  $\theta$  line, we set  $\rho = 0$  in the following calculations. Scaling-invariant combinations of the coupling constants are defined by

$$v = u_1 u_2, \quad w = u_0 u_2^3, \quad (4.2)$$

with fixed point values

$$v_* = 0.6567 (\varepsilon/6) + 2.9707 (\varepsilon/6)^2 + O(\varepsilon^3), \quad (4.3a)$$

$$w_* = 0.7052 (\varepsilon/6)^2 + O(\varepsilon^3). \quad (4.3b)$$

As it did for the swollen phase, the shift invariance leads to Ward identities for the collapse transition. Here, however, these Ward identities do not result in a scaling relation between the polymer exponents  $\theta$  and  $\nu_p$ , but they, nevertheless, simplify the calculations or provide consistency checks. The  $\varepsilon$  expansions for these exponents are

$$\theta = \frac{5}{2} - 0.4925(\varepsilon/6) - 0.5778(\varepsilon/6)^2, \quad (4.4a)$$

$$\nu_p = \frac{1}{4} + 0.1915(\varepsilon/6) + 0.0841(\varepsilon/6)^2. \quad (4.4b)$$

##### B. Calculation of the dynamical scaling exponent of collapsing randomly branched polymers

For our dynamical calculation, we complete the renormalization scheme, Eq. (4.1), by setting

$$s \rightarrow \hat{s} = Z^{1/2}(s + K\tilde{\varphi}), \quad (4.5a)$$

$$\tilde{s} \rightarrow \hat{\tilde{s}} = Z_\lambda Z^{1/2} \tilde{s}, \quad \lambda \rightarrow \hat{\lambda} = Z_\lambda^{-1} \lambda. \quad (4.5b)$$

Let us first describe the one-loop part of our calculation. Diagram (1) in Fig. 7 leads to the following contribution to the self-energy expanded to first order in  $\omega$  and  $\tau$ :

$$\begin{aligned} (1)_c &= -2\lambda g_1 g_2 \int_{\mathbf{p}} \frac{1}{(i\omega/\lambda + \tau + \mathbf{p}^2)(\tau + (\mathbf{q} - \mathbf{p})^2)} \\ &= -2\lambda g_1 g_2 \int_{\mathbf{p}} \left\{ \frac{1}{(\mathbf{p} - \mathbf{q})^2 \mathbf{p}^2} - \frac{i\omega/\lambda + \tau}{(\mathbf{p} - \mathbf{q})^2 (\mathbf{p}^2)^2} \right. \\ &\quad \left. - \frac{\tau}{\mathbf{p}^2 ((\mathbf{p} - \mathbf{q})^2)^2} + \dots \right\}. \end{aligned} \quad (4.6)$$

The factor 2 stems from the two possible orientations of the propagator in diagram (1). Performing the integrations as described in Appendix B and carrying out an  $\varepsilon$  expansion about  $d = 6$ , we find the renormalized one-loop vertex function

$$\begin{aligned} \Gamma_{1,1}^{(1L)}(q, \omega) &= (Z Z_\lambda i\omega + Z_\tau \lambda \tau + Z \lambda q^2) \\ &\quad - \frac{2v}{3\varepsilon} (3i\omega + 6\lambda \tau + \lambda q^2) + \dots \end{aligned} \quad (4.7)$$

From this, we read off the one-loop renormalization factors

$$Z = 1 + \frac{2v}{3\varepsilon}, \quad Z_\tau = 1 + \frac{4v}{\varepsilon}, \quad Z_\lambda = 1 + \frac{4v}{3\varepsilon}, \quad (4.8)$$

with  $Z$  and  $Z_\tau$  as already known from Ref. [5].

Now we turn to the two-loop self-energy diagrams in Fig. 7. For details of the calculation, we refer to Appendix B. It encompasses the frame counter-terms shown in Fig. 12 for which we get the results compiled in Eq. (B3). From these, we obtain the following results for the counter-terms of the

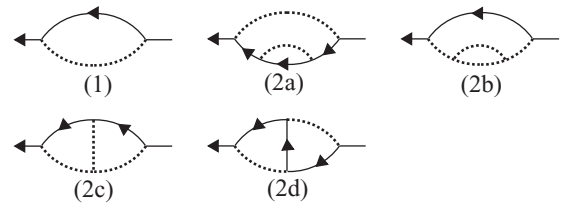


FIG. 7. Diagrams to two-loop order for the collapse transition. Dotted lines symbolize all possible arrangements of the static propagator including ghosts.

Feynman diagrams:

$$\begin{aligned} \mathcal{C}(2a)_c &= 4\lambda(g_1g_2)^2 \left\{ Ct(3,1,1) \right. \\ &\quad - (2Ct(3,2,1) + 3Ct(4,1,1))\tau \\ &\quad \left. - (Ct(3,2,1) + 2Ct(4,1,1))\frac{i\omega}{\lambda} \right\}, \end{aligned} \quad (4.9a)$$

$$\begin{aligned} \mathcal{C}(2b)_c &= \lambda(7(g_1g_2)^2 - g_0g_2^2) \left\{ Ct(3,1,1) \right. \\ &\quad - (2Ct(3,2,1) + 3Ct(4,1,1))\tau - Ct(4,1,1)\frac{i\omega}{\lambda} \left. \right\}, \end{aligned} \quad (4.9b)$$

$$\begin{aligned} \mathcal{C}(2c)_c &= \lambda(9(g_1g_2)^2 - g_0g_2^2) \left\{ Ct(2,2,1) \right. \\ &\quad - (4Ct(3,2,1) + Ct(2,2,2))\tau - 2Ct(3,2,1)\frac{i\omega}{\lambda} \left. \right\}, \end{aligned} \quad (4.9c)$$

$$\begin{aligned} \mathcal{C}(2d)_c &= 4\lambda(g_1g_2)^2 \left\{ Ct(2,2,1) \right. \\ &\quad - (4Ct(3,2,1) + Ct(2,2,2))\tau \\ &\quad \left. - (2Ct(3,2,1) + Ct(2,2,2))\frac{i\omega}{\lambda} \right\}. \end{aligned} \quad (4.9d)$$

These add up to

$$\begin{aligned} \mathcal{C}((2a) + \dots + (2d))_c &= \left[ \left( \frac{67}{18} - \frac{191}{216}\varepsilon \right) v^2 - \left( \frac{5}{18} - \frac{13}{216}\varepsilon \right) w \right] \frac{\lambda q^2}{\varepsilon^2} \\ &\quad + \left[ \left( \frac{63}{2} - \frac{301}{24}\varepsilon \right) v^2 - \left( \frac{5}{2} - \frac{23}{24}\varepsilon \right) w \right] \frac{\lambda \tau}{\varepsilon^2} \\ &\quad + \left[ \left( \frac{25}{2} - \frac{103}{24}\varepsilon \right) v^2 - \left( \frac{5}{6} - \frac{11}{72}\varepsilon \right) w \right] \frac{i\omega}{\varepsilon^2}. \end{aligned} \quad (4.10)$$

This defines the two-loop contributions to the renormalization factors  $Z$ ,  $Z_\tau$ , and  $ZZ_\lambda$ . Finally, we obtain

$$Z = 1 + \frac{2v}{3\varepsilon} + \frac{1}{\varepsilon^2} \left[ \left( \frac{67}{18} - \frac{191}{216}\varepsilon \right) v^2 - \left( \frac{5}{18} - \frac{13}{216}\varepsilon \right) w \right], \quad (4.11a)$$

$$Z_\tau = 1 + \frac{4v}{\varepsilon} + \frac{1}{\varepsilon^2} \left[ \left( \frac{63}{2} - \frac{301}{24}\varepsilon \right) v^2 - \left( \frac{5}{2} - \frac{23}{24}\varepsilon \right) w \right], \quad (4.11b)$$

$$ZZ_\lambda = 1 + \frac{4v}{3\varepsilon} + \frac{1}{\varepsilon^2} \left[ \left( \frac{83}{9} - \frac{92}{27}\varepsilon \right) v^2 - \left( \frac{5}{9} - \frac{5}{24}\varepsilon \right) w \right]. \quad (4.11c)$$

As they should be, the first two are in conformity with the results of Ref. [5]. The dynamic RG function becomes

$$\zeta = \left. \frac{\partial \ln Z_\lambda}{\partial \ln \mu} \right|_0 = -\frac{4v}{3} + \left( \frac{184}{27}v^2 - \frac{5}{12}w \right) + O(3\text{-loop}). \quad (4.12)$$

Using the fixed point values of the coupling constant given in Eq. (4.3), we obtain the  $\varepsilon$  expansion of the dynamic exponent

TABLE III. Estimates of the fractal dimensions of collapsing RBPs obtained via rational approximations.

$d$	1	2	3	4	5	6
$d_w$	2	3.038	3.882	4.631	5.332	6
$d_{\min}$	1	1.192	1.396	1.612	1.824	2
$d_f$	1	1.846	2.486	3.019	3.508	4

and, by the same token, the scaling dimension of the minimal path:

$$\begin{aligned} d_{\min} &= z = 2 + \zeta_* \\ &= 2 - 0.8756(\varepsilon/6) - 1.3162(\varepsilon/6)^2 + O(\varepsilon^3). \end{aligned} \quad (4.13)$$

Taking into account the exact values  $z = \nu_P = 1$  for  $d = 1$  ( $\varepsilon = 5$ ), we propose the rational approximations

$$d_{\min} = z \approx 2 - 0.14593\varepsilon \frac{1 + 0.726717\varepsilon}{1 + 0.476179\varepsilon} \quad (4.14)$$

and

$$1/d_f = \nu_P \approx \frac{1}{4} + \frac{0.0319167\varepsilon}{1 - 0.0733194\varepsilon - 0.016825\varepsilon^2}, \quad (4.15)$$

the latter being based on the  $\varepsilon$  expansion of  $\nu_P$  as given in Eq. (4.4). Table III lists the numerical values resulting from these rational approximations for various spatial dimension.

## V. CONCLUDING REMARKS

In summary, we have studied diffusion and transport on swollen and collapsing RBPs using renormalized dynamical field theory. In particular, we have calculated the diffusion exponent and a set of transport exponents including the fractal dimension of the minimal path and the resistance exponent to two-loop order. For the swollen polymer, our results are an improvement on the previously known one-loop results. For the collapse transition, our results are entirely new in the sense that, hitherto, no results beyond mean-field theory existed.

From a conceptual or diagrammatic standpoint, it is interesting to see that the dynamical Feynman diagrams for the self-energy decompose into a dynamic part, which has the form of a SAW connecting the external legs, and a residual quasistatic part. This observation simplifies the calculation of the dynamical renormalization enough to enable us to treat the problem to two-loop order.

As far as we know, the existing numerical results for diffusion and transport on substrates in the universality class of swollen RBPs and lattice animals are more than 25 years old. For the collapse transition, no such results exist. We hope that our results encourage simulation work leading to improved and extended numerical results.

## ACKNOWLEDGMENT

This work was supported in part by Grant No. NSF-DMR-1104707 to O.S.

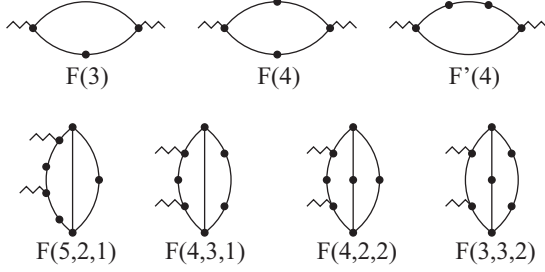


FIG. 8. Frames of the diagrams for swollen RBPs up to two-loop order.

### APPENDIX A: TWO-LOOP MASSLESS CALCULATION OF FRAMES AND COUNTER-TERMS NEAR $d = 8$

Here, we calculate the frames of the dynamical diagrams for the swollen phase using dimensional regularization [31]. We consider only those frames that are required to determine the dynamic renormalization factor to two-loop order. The calculation can be greatly simplified via the consequent use of massless propagators [32]. Of course, massless propagators bring about the danger of IR singularities, which would require the introduction of IR counter-terms [33,34] if they indeed occurred. However, cleverly using IR rearrangements of external momenta [35,36], the IR singularities can be avoided at least up to three-loop order. Figure 8 lists the massless frames that we need for our two-loop calculation. The wiggly lines symbolize external momenta  $\pm \mathbf{q}$  flowing into or out of the frame. These wiggly lines are positioned so that the frames are free of IR singularities.

First, let us return to the one-loop part of our calculation sketched in Sec. III. Equation (3.11) for diagram (1) can be expressed as

$$(1) = 2\lambda g^2 \{-G_d(1,2) + G_d(2,2)(i\omega/\lambda + \tau) + G_d(1,3)2\tau + \dots\}, \quad (\text{A1})$$

where  $G_d(\dots)$  is defined through the fundamental integral

$$\int_{\mathbf{p}} \frac{1}{(\mathbf{p}^2)^{\lambda_1} ((\mathbf{p} - \mathbf{q})^2)^{\lambda_2}} = G_d(\lambda_1, \lambda_2) q^{d-2(\lambda_1+\lambda_2)}. \quad (\text{A2})$$

This integral can be easily carried out using standard methods, with the result

$$G_d(\lambda_1, \lambda_2) = \frac{\Gamma(d/2 - \lambda_1)\Gamma(d/2 - \lambda_2)\Gamma(\lambda_1 + \lambda_2 - d/2)}{(4\pi)^{d/2}\Gamma(\lambda_1)\Gamma(\lambda_2)\Gamma(d - \lambda_1 - \lambda_2)}. \quad (\text{A3})$$

$\varepsilon$  expansion in  $\varepsilon = 8 - d$  leads to

$$F(3) = G_d(1,2)q^{2-\varepsilon} = -q^2 \frac{(\mu/q)^\varepsilon}{6\varepsilon} \left(1 + \frac{4}{3}\varepsilon + \dots\right) G_\varepsilon \mu^{-\varepsilon}, \quad (\text{A4a})$$

$$F(4) = G_d(1,3)q^{-\varepsilon} = \frac{(\mu/q)^\varepsilon}{3\varepsilon} \left(1 + \frac{13}{12}\varepsilon + \dots\right) G_\varepsilon \mu^{-\varepsilon}, \quad (\text{A4b})$$

$$F'(4) = G_d(2,2)q^{-\varepsilon} = \frac{(\mu/q)^\varepsilon}{3\varepsilon} \left(1 + \frac{5}{6}\varepsilon + \dots\right) G_\varepsilon \mu^{-\varepsilon}, \quad (\text{A4c})$$

with  $G_\varepsilon = \Gamma(1 + \varepsilon/2)/(4\pi)^{d/2}$ . Note that for these values of the parameters  $\lambda_i$ , integral (A2) does not contain IR singularities. Hence, the  $\varepsilon$  poles in Eqs. (A4) arise purely from UV singularities as they should, i.e., we have successfully avoided IR singularities even though we resorted to massless propagators.

Next, we consider the two-loop diagrams. Frames with the arrangement of external momenta as shown in Fig. 8 are free of IR singularities. They are easily integrated through a successive application of Eq. (A2). We obtain

$$F(5,2,1) = G_d(2,6-d/2)G_d(1,2)q^{-2\varepsilon} = -\frac{(\mu/q)^{2\varepsilon}}{36\varepsilon^2} \left(1 + \frac{25}{12}\varepsilon + \dots\right) G_\varepsilon^2 \mu^{-2\varepsilon}, \quad (\text{A5a})$$

$$F(4,3,1) = G_d(2,6-d/2)G_d(1,3)q^{-2\varepsilon} = \frac{(\mu/q)^{2\varepsilon}}{18\varepsilon^2} \left(1 + \frac{11}{6}\varepsilon + \dots\right) G_\varepsilon^2 \mu^{-2\varepsilon}, \quad (\text{A5b})$$

$$F(4,2,2) = G_d(2,6-d/2)G_d(2,2)q^{-2\varepsilon} = \frac{(\mu/q)^{2\varepsilon}}{18\varepsilon^2} \left(1 + \frac{19}{12}\varepsilon + \dots\right) G_\varepsilon^2 \mu^{-2\varepsilon}, \quad (\text{A5c})$$

$$F(3,3,2) = G_d(1,7-d/2)G_d(2,3)q^{-2\varepsilon} = \frac{(\mu/q)^{2\varepsilon}}{24\varepsilon} \left(1 + \dots\right) G_\varepsilon^2 \mu^{-2\varepsilon}. \quad (\text{A5d})$$

Now we calculate the counter-terms using a BPHZ type of renormalization [35,37], i.e., a recursive renormalization procedure defined by a sequence of operative steps. To this end, we define a pole-separating procedure  $\mathfrak{P}$  operating on  $\varepsilon$  expansions:

$$\mathfrak{P} \sum_{i=-\infty}^{\infty} c_i \varepsilon^i = \sum_{i=-\infty}^{-1} c_i \varepsilon^i. \quad (\text{A6})$$

The counter-terms are constructed by the operation

$$\mathfrak{C} = \mathfrak{P}\mathfrak{R}', \quad (\text{A7})$$

where the incomplete renormalization  $\mathfrak{R}'$  operates on the momentum integrals  $I_\Gamma$  of the one-particle irreducible diagrams  $\Gamma$ . It is recursively defined by

$$\mathfrak{R}' I_\Gamma = I_\Gamma + \sum_{\{\gamma\} \in D_\Gamma} I_{\Gamma/\{\gamma\}} \cdot \prod_{\gamma_i \in \{\gamma\}} (-\mathfrak{C} I_{\gamma_i}). \quad (\text{A8})$$

Here  $D_\Gamma$  is the set of all collections  $\{\gamma\} = \{\gamma_1, \gamma_2, \dots\}$  of disjoint superficially divergent one-particle irreducible subdiagrams  $\gamma_i$  of  $\Gamma$ , and  $\Gamma/\{\gamma\}$  is the diagram obtained from  $\Gamma$  by collapsing each of these subdiagrams to points. Applying  $\mathfrak{R}'$  to a superficially convergent diagram  $\Gamma$ ,  $\mathfrak{R}' I_\Gamma$  is finite for  $\varepsilon \rightarrow 0$ , and  $\mathfrak{C} I_\Gamma = 0$ . The operation  $\mathfrak{R}'$  applied to superficially divergent diagrams produces poles in  $\varepsilon$  with coefficients polynomial in the external momenta and internal masses without nonprimitive logarithmic terms. Finally, the operation  $\mathfrak{C} I_\Gamma$  yields the wanted counter-terms, and the complete renormalization  $\mathfrak{R} I_\Gamma = \mathfrak{R}' I_\Gamma - \mathfrak{C} I_\Gamma = (1 - \mathfrak{P})\mathfrak{R}' I_\Gamma$  leads to a finite result.

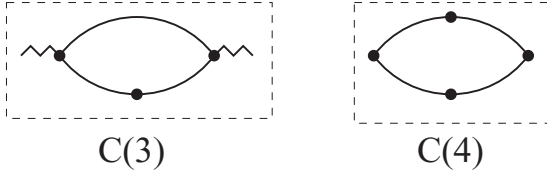


FIG. 9. One-loop counter-terms in  $d = 8 - \varepsilon$  dimensions.

Of course, applying  $\mathfrak{R}'$  to one-loop diagrams is trivial. The counter-terms (dashed boxes) are shown in Fig. 9. Using Eqs. (A4), we get

$$C(3) = \mathfrak{P}F(3) = -\frac{G_\varepsilon \mu^{-\varepsilon}}{6\varepsilon} q^2, \quad (\text{A9a})$$

$$C(4) = \mathfrak{P}F(4) = \mathfrak{P}F'(4) = \frac{G_\varepsilon \mu^{-\varepsilon}}{3\varepsilon}. \quad (\text{A9b})$$

Note that we leave factors  $G_\varepsilon \mu^{-\varepsilon}$  unexpanded because they are absorbed by the dimension-bearing coupling constants [cf. the renormalization scheme, Eq. (3.3)]. Note also that because of the application of the operation  $\mathfrak{C}$ , it does not matter at which vertices we have injected the external momenta as IR regulators into a given superficially logarithmically divergent diagram  $\Gamma$  as long as IR divergencies are avoided.

At two-loop order, the procedure  $\mathfrak{P}$  produces the counter-terms listed in Fig. 10. Mathematically, these stand for

$$\begin{aligned} C(5,2,1) &= \mathfrak{P}[F(5,2,1) - G_d(2,2)C(3)] \\ &= \mathfrak{P}\left\{-\frac{(\mu/q)^{2\varepsilon}}{36\varepsilon^2}\left(1 + \frac{25}{12}\varepsilon\right) + \frac{(\mu/q)^\varepsilon}{18\varepsilon^2}\left(1 + \frac{5}{6}\varepsilon\right)\right\}(G_\varepsilon \mu^{-\varepsilon})^2 \\ &= \frac{(G_\varepsilon \mu^{-\varepsilon})^2}{36\varepsilon^2}\left(1 - \frac{5}{12}\varepsilon\right), \quad (\text{A10a}) \end{aligned}$$

$$\begin{aligned} C(4,3,1) &= \mathfrak{P}[F(4,3,1) - G_d(2,2)C(4)] \\ &= \mathfrak{P}\left\{\frac{(\mu/q)^{2\varepsilon}}{18\varepsilon^2}\left(1 + \frac{11}{6}\varepsilon\right)\right\} \end{aligned}$$

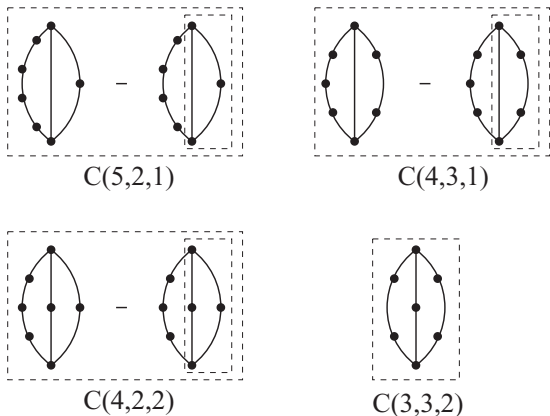


FIG. 10. Two-loop counter-terms in  $d = 8 - \varepsilon$  dimensions.

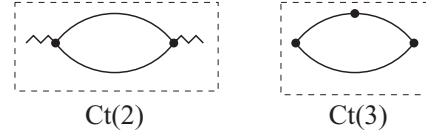


FIG. 11. One-loop counter-terms in  $d = 6 - \varepsilon$  dimensions.

$$\begin{aligned} &-\frac{(\mu/q)^\varepsilon}{9\varepsilon^2}\left(1 + \frac{5}{6}\varepsilon\right)\}(G_\varepsilon \mu^{-\varepsilon})^2 \\ &= -\frac{(G_\varepsilon \mu^{-\varepsilon})^2}{18\varepsilon^2}\left(1 - \frac{1}{6}\varepsilon\right), \quad (\text{A10b}) \end{aligned}$$

$$\begin{aligned} C(4,2,2) &= \mathfrak{P}[F(4,2,2) - G_d(2,2)C(4)] \\ &= \mathfrak{P}\left\{\frac{(\mu/q)^{2\varepsilon}}{18\varepsilon^2}\left(1 + \frac{19}{12}\varepsilon\right) - \frac{(\mu/q)^\varepsilon}{9\varepsilon^2}\left(1 + \frac{5}{6}\varepsilon\right)\right\} \\ &= -\frac{(G_\varepsilon \mu^{-\varepsilon})^2}{18\varepsilon^2}\left(1 + \frac{1}{12}\varepsilon\right), \quad (\text{A10c}) \end{aligned}$$

$$C(3,3,2) = \mathfrak{P}[F(3,3,2)] = \frac{(G_\varepsilon \mu^{-\varepsilon})^2}{24\varepsilon}. \quad (\text{A10d})$$

### APPENDIX B: TWO-LOOP CALCULATION AND COUNTER-TERMS NEAR $d = 6$

The counter-terms needed for the collapse transition (see Figs. 11 and 12) can be obtained through a massless calculation using methods similar to those explained in Appendix A in conjunction with t'Hooft and Veltman's "partial  $p$ " method [31]. Partially, they can also be extracted from results of de Alcantara Bonfim *et al.* [29] for the usual  $\phi^3$ -field theory.

Let us start here by revisiting Eq. (4.6). In terms of the fundamental integral, Eq. (A2), this one-loop diagram can be

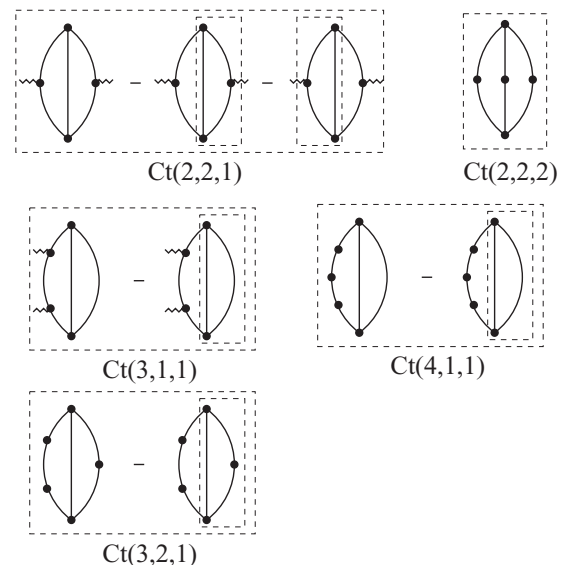


FIG. 12. Two-loop counter-terms in  $d = 6 - \varepsilon$  dimensions.

expressed as

$$(1)_c = 2\lambda g_1 g_2 \{-G_d(1,1) + G_d(2,1)(i\omega/\lambda + 2\tau) + \dots\}. \quad (\text{B1})$$

After  $\varepsilon$  expansion about  $d = 6$ , we extract the counter-terms

$$Ct(2) = -\frac{G_\varepsilon \mu^{-\varepsilon}}{3\varepsilon} q^2, \quad Ct(3) = \frac{G_\varepsilon \mu^{-\varepsilon}}{\varepsilon}. \quad (\text{B2})$$

For the two-loop counter-terms, we obtain

$$Ct(2,2,1) = \frac{(G_\varepsilon \mu^{-\varepsilon})^2}{3\varepsilon^2} \left(1 - \frac{1}{3}\varepsilon\right) q^2, \quad (\text{B3a})$$

$$Ct(3,1,1) = -\frac{(G_\varepsilon \mu^{-\varepsilon})^2}{18\varepsilon^2} \left(1 - \frac{11}{12}\varepsilon\right) q^2, \quad (\text{B3b})$$

$$Ct(4,1,1) = \frac{(G_\varepsilon \mu^{-\varepsilon})^2}{6\varepsilon^2} \left(1 - \frac{7}{12}\varepsilon\right), \quad (\text{B3c})$$

$$Ct(3,2,1) = -\frac{(G_\varepsilon \mu^{-\varepsilon})^2}{2\varepsilon^2} \left(1 - \frac{1}{4}\varepsilon\right), \quad (\text{B3d})$$

$$Ct(2,2,2) = \frac{(G_\varepsilon \mu^{-\varepsilon})^2}{2\varepsilon}. \quad (\text{B3e})$$

### APPENDIX C: RELATIONS BETWEEN FEYNMAN INTEGRALS IN $d$ AND $(d - 2)$ DIMENSIONS

It is well known that supersymmetry relates many Feynman integrals with insertions to the corresponding integrals in two lesser dimensions [4,38]. Therefore, the question arises whether such relations can be used to determine the counter-terms of the frames needed in our dynamical calculation. We show explicitly that this indeed is the case, at least to two-loop order. This observation may open the route to a three-loop calculation since all counter-terms near  $d = 6$  are known [29]. For background information on the following reasoning, see the textbook by Itzykson and Zuber [37].

Consider a one-particle irreducible Feynman diagram  $G$  without tadpoles consisting of  $V$  vertices,  $I$  internal lines, and  $L = I - V + 1$  loops in  $d$  dimensions. Each line  $l$  carries a propagator  $1/(\tau_l + \mathbf{q}_l^2)$ , where  $\mathbf{q}_l$  is a  $d$ -dimensional momentum vector, and  $\tau_l$  an auxiliary mass squared, which is finally set to 0 in a massless calculation. Next, let us introduce an (arbitrary) orientation of each line, and we define the incidence matrix  $(\varepsilon_{vl})$ ,

$$\varepsilon_{vl} = \begin{cases} 1 & \text{if the vertex } v \text{ is the starting point of line } l, \\ -1 & \text{if the vertex } v \text{ is the endpoint of line } l, \\ 0 & \text{if } l \text{ is not incident on } v. \end{cases} \quad (\text{C1})$$

Momentum conservation at each vertex  $v$  is expressed as

$$\sum_{l=1}^I \varepsilon_{vl} \mathbf{q}_l = \mathbf{Q}_v, \quad (\text{C2})$$

where  $\mathbf{Q}_v$  is the external momentum flowing into vertex  $v$ . Only  $(V - 1)$  of the conservation laws, Eq. (C2), are

independent since

$$\sum_{v=1}^V \varepsilon_{vl} = 0. \quad (\text{C3})$$

The last one produces the overall conservation

$$\sum_{v=1}^V \mathbf{Q}_v = 0. \quad (\text{C4})$$

The contribution  $I(G, \{\mathbf{Q}_v\})_d$  of diagram  $G$  to the corresponding vertex function can be written in a Schwinger parametric form as [37]

$$I(G, \{\mathbf{Q}_v\})_d = \int_0^\infty \prod_{l=1}^I ds_l \int_{\{\mathbf{q}\}} \exp\left(-\sum_l (\tau_l + \mathbf{q}_l^2) s_l\right) \times \prod_{v=1}^{V-1} \left( (2\pi)^d \delta^{(d)}\left(\sum_l \varepsilon_{vl} \mathbf{q}_l - \mathbf{Q}_v\right) \right), \quad (\text{C5})$$

where we focus on the diagram's frame (integral over the loop momenta) and omit any symmetry factors and coupling constants. Using the integral representation of the  $\delta$  functions and performing all the arising Gaussian integration, we arrive at

$$I(G, \{\mathbf{Q}_v\})_d = \int_0^\infty \prod_{l=1}^I (e^{-\tau_l s_l} ds_l) \times \frac{\exp(-\mathcal{Q}(\{s_l\}, \{\mathbf{Q}_v\})/\mathcal{P}(\{s_l\}))}{((4\pi)^L \mathcal{P}(\{s_l\}))^{d/2}}. \quad (\text{C6})$$

Here,  $\mathcal{P}(\{s_l\})$  is given by

$$\mathcal{P}(\{s_l\}) = (4\pi)^{-L} \prod_{l=1}^I (4\pi s_l) \frac{\det A}{(4\pi)^{V-1}}. \quad (\text{C7})$$

$A$  is the  $(V - 1) \times (V - 1)$  matrix with elements  $A_{vv'} = \sum_l \varepsilon_{vl} s_l^{-1} \varepsilon_{v'l}$ , where  $v, v' = 1, \dots, V - 1$ .  $\mathcal{Q}(\{s_l\}, \{\mathbf{Q}_v\})$  is the bilinear form constructed from the  $\{\mathbf{Q}_v\}$  and the inverse of the matrix  $A$ :

$$\mathcal{Q}(\{s_l\}, \{\mathbf{Q}_v\}) = \mathcal{P}(\{s_l\}) \sum_{v,v'=1}^{V-1} \mathbf{Q}_v \cdot (A^{-1})_{vv'} \mathbf{Q}_{v'}. \quad (\text{C8})$$

$\mathcal{P}$  and  $\mathcal{Q}$  are readily simplified using Kirchhoff's laws on linear electrical networks [39]:

$$\mathcal{P}(\{s_l\}) = \sum_T \prod_{l \notin T} s_l, \quad (\text{C9a})$$

$$\mathcal{Q}(\{s_l\}, \{\mathbf{Q}_v\}) = \sum_{(T_1, T_2)} \prod_{l \notin T_1, T_2} s_l \left( \sum_{v \in T_1} \mathbf{Q}_v \right)^2. \quad (\text{C9b})$$

Here, the sum  $T$  runs over all spanning trees, and the sum  $(T_1, T_2)$  runs over all pairs of mutually disconnected spanning trees (a forest with two trees) in diagram  $G$ , respectively. Note that the dependence of  $I(G, \{\mathbf{Q}_v\})_d$ , as given in Eq. (C5), on the dimensionality  $d$  rests entirely in the exponent of the denominator.

Now let us define the procedure

$$T^* = (4\pi)^L \mathcal{P}(\{-\partial/\partial\tau_l\}), \quad (C10)$$

which produces the sum over all diagrams obtained by inserting  $s^2$  into all lines of  $G$  not belonging to any tree. Applying this procedure to  $I(G, \{\mathbf{Q}_v\})_d$  transforms this integral into its  $(d - 2)$ -dimensional counterpart:

$$T^* I(G, \{\mathbf{Q}_v\})_d = I(T^* G, \{\mathbf{Q}_v\})_d = I(G, \{\mathbf{Q}_v\})_{d-2}. \quad (C11)$$

Next, we turn to the self-energy diagrams in  $d$  dimensions. These diagrams have only two external momenta,  $\{\mathbf{Q}_v\} = \{\mathbf{q}, -\mathbf{q}\}$ , and the bilinear form  $\mathcal{Q}(\{s_l\}, \{\mathbf{Q}_v\})$  can contain only those partitions into two disconnected trees  $(T_1, T_2)$  that disconnect the two external vertices where the external momenta enter or exit the diagram. The product  $\prod_{l \notin T_1, T_2} s_l$  therefore runs over the  $L + 1$  lines that belong to a cut set which divides the diagram into two tree-like subdiagrams, each containing one external vertex. In this case, the form  $\mathcal{Q}(\{s_l\}, \{\mathbf{Q}_v\})$  reduces to

$$\mathcal{Q}(\{s_l\}, \{\mathbf{Q}_v\}) = \sum_{(T_1, T_2)} \prod_{l \notin T_1, T_2} s_l \mathbf{q}^2 =: \mathcal{Q}^*(\{s_l\}) \mathbf{q}^2, \quad (C12)$$

where  $v_1 \in T_1$  and  $v_2 \in T_2$ . Now we define the procedure

$$C^* = (4\pi)^L \mathcal{Q}^*(\{-\partial/\partial\tau_l\}), \quad (C13)$$

which produces the sum over all diagrams obtained from  $G$  by placing an insertion into any of its cut-set lines. Applying this

procedure to  $I(G, \{\mathbf{q}, -\mathbf{q}\})_d$  results in

$$\begin{aligned} C^* I(G, \{\mathbf{q}, -\mathbf{q}\})_d &= I(C^* G, \{\mathbf{q}, -\mathbf{q}\})_d \\ &= -\frac{\partial}{\partial \mathbf{q}^2} I(G, \{\mathbf{q}, -\mathbf{q}\})_{d-2}. \end{aligned} \quad (C14)$$

Note that this theorem relates quadratically diverging diagrams to logarithmic diverging diagrams in two dimensions higher.

Having derived theorems (C11) and (C14), we now can use them to extract relations between the counter-terms encountered in our two-loop calculations. Applying the  $T^*$  procedure, we obtain

$$\begin{aligned} Ct(2,2,2) &= 12C(3,3,2), \\ Ct(3,2,1) &= 6C(4,3,1) + 3C(4,2,2) + 2C(3,3,2), \\ Ct(4,1,1) &= 8C(5,2,1) + C(4,2,2). \end{aligned} \quad (C15)$$

The  $C^*$  procedure provides us with the relations

$$\begin{aligned} -\frac{\partial}{\partial \mathbf{q}^2} Ct(2,2,1) &= 4C(4,3,1) + 2C(4,2,2) + 2C(3,3,2), \\ -\frac{\partial}{\partial \mathbf{q}^2} Ct(3,1,1) &= 4C(5,2,1) + C(4,2,2). \end{aligned} \quad (C16)$$

These five relations determine all four two-loop counter-terms near eight dimensions from the five two-loop counter-terms near six dimensions and, in addition, provide us one supplementary consistency check for our calculations.

- 
- [1] P. G. de Gennes, *La Recherche* **7**, 919 (1976).
  - [2] S. Wilke, Y. Gefen, V. Ilkovic, A. Aharony, and D. Stauffer, *J. Phys. A: Math. Gen.* **17**, 647 (1984).
  - [3] T. C. Lubensky and J. Isaacson, *Phys. Rev. Lett.* **41**, 829 (1978); **42**, 410(E) (1978); *Phys. Rev. A* **20**, 2130 (1979).
  - [4] G. Parisi and N. Sourlas, *Phys. Rev. Lett.* **46**, 871 (1981).
  - [5] H. K. Janssen and O. Stenull, *Europhys. Lett.* **90**, 46003 (2010); *Phys. Rev. E* **83**, 051126 (2011).
  - [6] S. Havlin, Z. V. Djordjevic, I. Majid, H. E. Stanley, and G. H. Weiss, *Phys. Rev. Lett.* **53**, 178 (1984).
  - [7] S. Havlin and D. Ben-Avraham, *Adv. Phys.* **36**, 695 (1987).
  - [8] P. Grassberger, *Phys. Rev. E* **56**, 3682 (1997).
  - [9] H.-P. Hsu, W. Nadler, and P. Grassberger, *J. Phys. A: Math. Gen.* **38**, 775 (2005).
  - [10] H.-P. Hsu and P. Grassberger, *J. Stat. Phys.* **144**, 597 (2011).
  - [11] V. Blavatska and W. Janke, *Phys. Rev. Lett.* **101**, 125701 (2008); *Phys. Procedia* **3**, 1431 (2010).
  - [12] V. Blavatska and W. Janke, *Europhys. Lett.* **82**, 66006 (2008); **42**, 015001 (2009).
  - [13] D. Mollison, *J. R. Stat. Soc. B* **39**, 283 (1977).
  - [14] P. Grassberger, *Math. Biosci.* **63**, 157 (1983).
  - [15] H. K. Janssen, *Z. Phys. B: Cond. Matter* **58**, 311 (1985).
  - [16] J. L. Cardy and P. Grassberger, *J. Phys. A: Math. Gen.* **18**, L267 (1985).
  - [17] H. K. Janssen and U. C. Täuber, *Ann. Phys.* **315**, 147 (2005).
  - [18] H. K. Janssen, M. Müller, and O. Stenull, *Phys. Rev. E* **70**, 026114 (2004).
  - [19] D. Stauffer and A. Aharony, *Introduction to Percolation Theory* (Taylor and Francis, London, 1994).
  - [20] H. K. Janssen, *J. Phys. C: Cond. Matter* **17**, S1973 (2005).
  - [21] D. J. Amit, *Field Theory, the Renormalization Group, and Critical Phenomena* (World Scientific, Singapore, 1984).
  - [22] J. Zinn-Justin, *Quantum Field Theory and Critical Phenomena*, 4th ed. (Clarendon, Oxford, 2002).
  - [23] H. K. Janssen, *Z. Phys. B* **23**, 377 (1976); R. Bausch, H. K. Janssen, and H. Wagner, *ibid.* **24**, 113 (1976).
  - [24] C. De Dominicis, *J. Phys. C* **37**, 247 (1976); C. De Dominicis and L. Peliti, *Phys. Rev. B* **18**, 353 (1978).
  - [25] H. K. Janssen, in *Dynamical Critical Phenomena and Related Topics, Lecture Notes in Physics*, Vol. 104, edited by C. P. Enz (Springer, Heidelberg, 1979); in *From Phase Transition to Chaos*, edited by G. Györgyi, I. Kondor, L. Sasvári, and T. Tél (World Scientific, Singapore, 1992).
  - [26] N. Breuer and H. K. Janssen, *Z. Phys. B: Cond. Matter* **41**, 55 (1981).
  - [27] D. C. Brydges and J. Z. Imbrie, *Ann. Math.* **158**, 1019 (2003); *J. Stat. Phys.* **110**, 503 (2003).
  - [28] For a very clear pedagogical presentation of the work of Brydges and Imry, see J. Cardy, e-print [arXiv:cond-mat/0302495v3](https://arxiv.org/abs/cond-mat/0302495v3).
  - [29] O. F. de Alcantara Bonfim, J. E. Kirkham, and A. J. McKane, *J. Phys. A: Math. Gen.* **13**, L247 (1980); **14**, 2391 (1981).
  - [30] H. Gould and R. P. Kohin, *J. Phys. A: Math. Gen.* **17**, L159 (1984).

- [31] G. t'Hooft and M. Veltman, *Nucl. Phys. B* **44**, 189 (1972); G. t'Hooft, *ibid.* **61**, 455 (1973).
- [32] D. I. Kazakov, *Phys. Lett. B* **133**, 406 (1983); *Theor. Mat. Phys.* **62**, 84 (1985).
- [33] K. G. Chetyrkin and F. V. Tkachov, *Phys. Lett. B* **114**, 340 (1982).
- [34] K. G. Chetyrkin and V. A. Smirnov, *Phys. Lett. B* **144**, 419 (1984).
- [35] A. A. Vladimirov, *Theor. Mat. Phys.* **36**, 732 (1978); **43**, 417 (1980).
- [36] K. G. Chetyrkin, A. L. Kataev, and F. V. Tkachov, *Nucl. Phys. B* **174**, 345 (1980); *Phys. Lett. B* **99**, 147 (1981).
- [37] For a general reference to quantum field theoretic methods, see, e.g., C. Itzykson and J.-B. Zuber, *Quantum Field Theory* (McGraw-Hill, New York, 1980).
- [38] G. Parisi and N. Sourlas, *Phys. Rev. Lett.* **43**, 744 (1979).
- [39] G. Kirchhoff, *Ann. Phys. Chem.* **72**, 497 (1847).